Pulsatile Stimulation Determines Timing and Specificity of NF-κB–Dependent Transcription

Louise Ashall,[1]* Caroline A. Horton,[1]* David E. Nelson,[1]* Pawel Paszek,[1]* Claire V. Harper,[1] Kate Sillitoe,[1] Sheila Ryan,[1] David G. Spiller,[1] John F. Unitt,[2] David S. Broomhead,[3] Douglas B. Kell,[4] David A. Rand,[5] Violaine Sée,[1] Michael R. H. White[1]†

The nuclear factor κB (NF-κB) transcription factor regulates cellular stress responses and the immune response to infection. NF-κB activation results in oscillations in nuclear NF-κB abundance. To define the function of these oscillations, we treated cells with repeated short pulses of tumor necrosis factor–α at various intervals to mimic pulsatile inflammatory signals. At all pulse intervals that were analyzed, we observed synchronous cycles of NF-κB nuclear translocation. Lower frequency stimulations gave repeated full-amplitude translocations, whereas higher frequency pulses gave reduced translocation, indicating a failure to reset. Deterministic and stochastic mathematical models predicted how negative feedback loops regulate both the resetting of the system and cellular heterogeneity. Altering the stimulation intervals gave different patterns of NF-κB–dependent gene expression, which supports the idea that oscillation frequency has a functional role.

Eukaryotic cells interpret multiple signals to coordinate the activity of transcription factors, which modulate the expression of target genes. Nuclear factor κB (NF-κB) signaling in many mammalian cell types regulates responses to pathogens and stresses (*1*). NF-κB, most commonly comprising a dimer of RelA and p50, is bound in the cytoplasm of unstimulated cells by inhibitor of nuclear factor κB (IκB) proteins. Stimulation by cytokines such as tumor necrosis factor–α (TNFα) activates the IκB kinase (IKK) complex that phosphorylates IκB proteins, leading to IκB degradation and NF-κB translocation into the nucleus. Activated NF-κB regulates transcription from promoter regions of approximately 300 genes, including those encoding cytokines and several NF-κB family members that can feedback to regulate the system (*2*). Signaling through NF-κB can regulate diverse cellular outcomes, including cell death or division (*3*). How such a diversity of responses is generated has remained unclear.

Real-time fluorescence imaging and mathematical modeling have shown that the activity of the NF-κB system can be oscillatory (*4*). This raised the possibility that, such as with calcium (*5*), this signaling pathway might use oscillation frequency as one component of the cellular signal that controls innate immunity and cell fate. After stimulation with TNFα, target gene expression can be regulated by negative feedback loops that modulate the cytoplasmic-nuclear translocation of NF-κB (*4*). One of these feedbacks is mediated by IκBα, which upon binding to NF-κB in the nucleus shuttles the NF-κB protein complex back to the cytoplasm. These oscillations have been observed in single cells expressing the fluorescently labeled NF-κB subunit RelA and IκBα (*4*, *6*, *7*) and also through bulk cell electrophoretic mobility shift assay (EMSA) analysis in IκBε and IκBε-IκBβ knockout mouse embryonic fibroblasts (MEFs) (*8*, *9*).

Single-live-cell fluorescent imaging has demonstrated NF-κB oscillations in various cell types (*4*, *6*). SK-N-AS neuroblastoma cells showed particularly robust oscillations in response to TNFα simulation after transient (*4*) or stable transfection with a vector expressing RelA fused to the *Discosoma sp.* red fluorescent protein dsRed-Express (RelA-dsRedxp) (Fig. 1, A and B). Oscillations were unlikely to be the result of RelA overexpression, because stably transfected cells expressed nearly physiological amounts of the fusion protein [relative level of 0.91 ± 0.04 (SD, $n = 6$ replicates) compared with endogenous protein in untransfected control (*7*)]. In contrast to the conclusions of other reports (*9*, *10*), we observed oscillations in the translocation of RelA-dsRedxp fusion protein in single transiently transfected MEFs (Fig. 1, C to E). These data [as well as bulk cell chromatin immunoprecipitation (ChIP) assays (fig. S1)] suggest that oscillations are a normal response to TNFα stimulation.

In an inflammatory tissue, cells receive pulsatile signals such as TNFα from neighboring cells

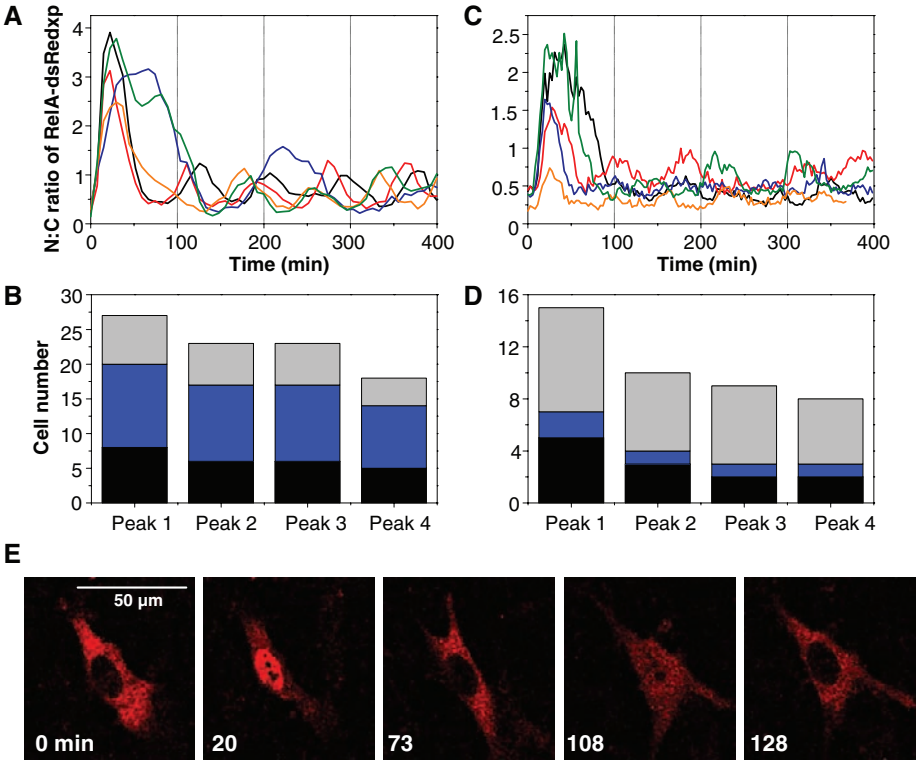

Fig. 1. RelA oscillations at the single-cell level. (**A** and **C**) Time course of the ratio of nuclear to cytoplasmic localization (N:C) of RelA-dsRedxp in (A) SK-N-AS (stably transfected) and (C) MEF (transiently transfected) cells. Single-cell dynamics are shown by differently colored lines. (**B** and **D**) The number of cells (separate experiments are represented by different colors) showing RelA-dsRedxp translocations in (B) stably transfected SK-N-AS (imaged for at least 350 min; 0 cells failed to respond) and (D) transiently transfected MEF cells (imaged for at least 250 min; 1 cell failed to respond). (**E**) Time-lapse confocal images of a typical RelA-dsRedxp-transfected MEF cell after TNFα stimulation.

[1]Centre for Cell Imaging, School of Biological Sciences, Bioscience Research Building, Crown Street, Liverpool, L69 7ZB, UK. [2]Molecular Biology Department, AstraZeneca R&D Charnwood, Bakewell Road, Loughborough, Leicestershire, LE11 5RH, UK. [3]School of Mathematics, The Alan Turing Building, The University of Manchester, Oxford Road, Manchester, M13 9PL, UK. [4]Manchester Centre for Integrative Systems Biology, School of Chemistry, and Manchester Interdisciplinary Biocentre, University of Manchester, 131 Princess Street, Manchester, M1 7DN. [5]Warwick Systems Biology, Coventry House, University of Warwick, Coventry CV4 7AL, UK.

*These authors contributed equally to this work.
†To whom correspondence should be addressed. E-mail: mwhite@liv.ac.uk

(*11*, *12*). To mimic this, we exposed cells to 5-min pulses of TNFα at various intervals, followed by a wash-off. When stimulated at 200-min intervals, RelA-dsRedxp fusion protein expressed in SK-N-AS cells showed synchronous translocations from the cytoplasm to the nucleus and back of equal magnitude in response to each successive pulse (Fig. 2, A and B, and fig. S4). In contrast, whereas stimulation at 100- or 60-min intervals also caused synchronous cell responses, there was significant reduction in the magnitude of RelA-dsRedxp fusion protein translocation (Fig. 2, A and B). These data indicate that the system completely resets between 100 and 200 min after each stimulus. Western blot analysis of synchronized cell populations supported the hypothesis that the cycles of RelA-dsRedxp fusion protein translocation were associated with cycles of phosphorylation at Ser^{32} and degradation of IκBα (Fig. 2C and fig. S5). Analysis of the amounts of Ser^{32}-phospho-IκBα, relative to total IκBα levels, confirmed that the failure to reset was quantitatively reflected by the phosphorylation of IκBα (Fig. 2, C and D, and fig. S6). Cycles of phosphorylation and dephosphorylation of RelA at Ser^{536} were consistent with RelA being phosphorylated in the cytoplasm and dephosphorylated in the nucleus (*4*).

The inability of available model structures (*7*, *8*, *13*, *14*) to provide a single parameter set that could simulate the observed behavior for all

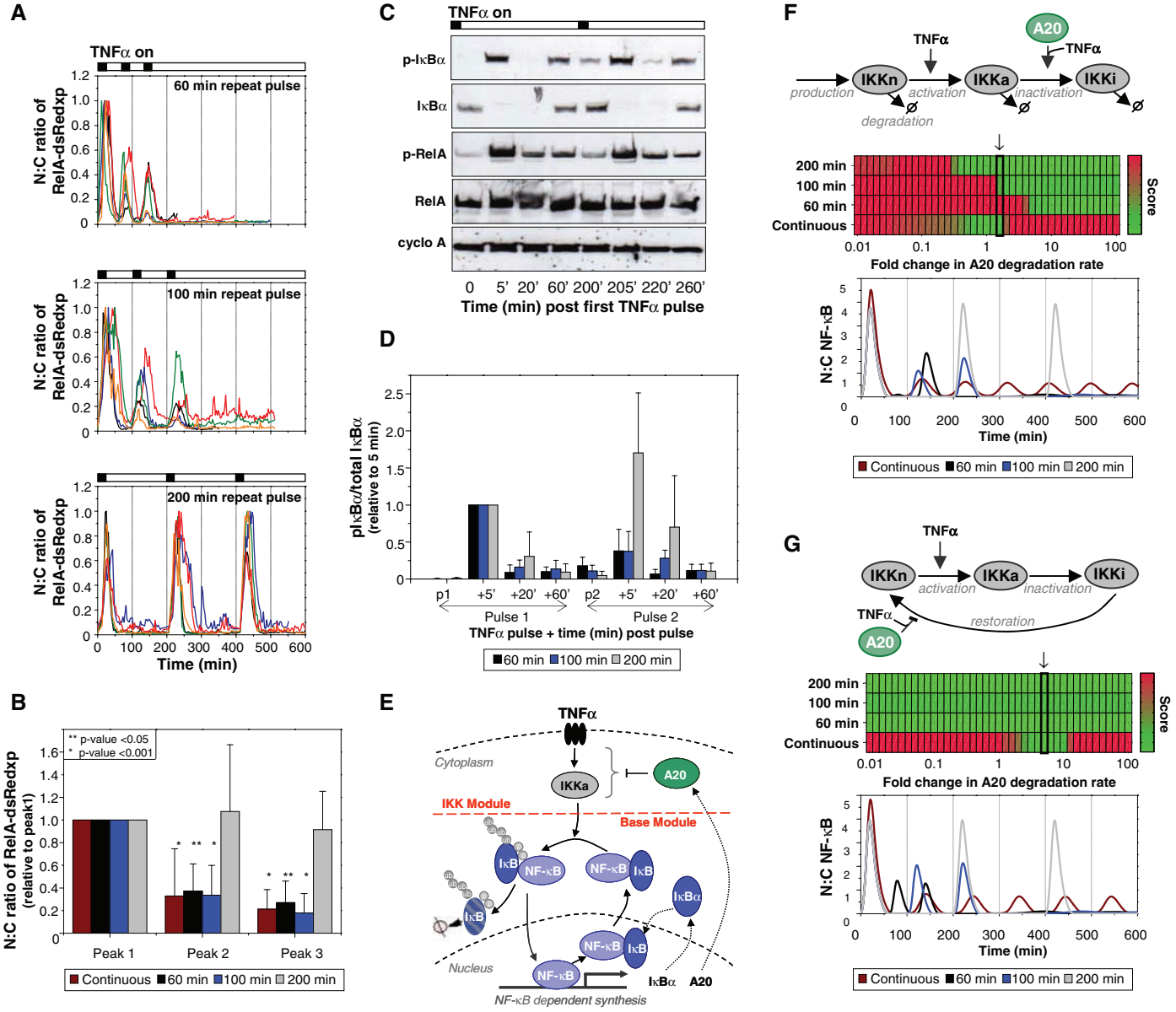

Fig. 2. Response of SK-N-AS cells to various TNFα pulse frequencies. (**A**) Time course of RelA-dsRedxp N:C ratio in transiently transfected cells pulsed three times with TNFα for 5 min at intervals of 60, 100, or 200 min (five typical cells shown for each). RelA-dsRedxp N:C ratio was normalized to peak 1 intensity. (**B**) Amplitude of successive peaks of RelA-dsRedxp localization after pulses or continuous exposure of cells to TNFα. Results were normalized to the amplitude of peak 1 (+SD). Asterisks indicate *P* values for a one-sample Wilcoxon test for peak amplitude equal to 1. (**C**) Western blot of Ser^{32} phospho-IκBα (p-IκBα), IκBα, Ser^{536} phospho-RelA (p-RelA), RelA, and cyclophilin A (cyclo A) amounts in cells stimulated with TNFα pulses 200 min apart. (**D**) Ratio of p-IκBα/total IκBα (relative to that recorded at t = 5 min) in cells stimulated 60, 100, and 200 min apart (+SD) [data based on (C)] (fig. S4). p1 and p2 indicate time after pulse 1 or 2 for each stimulation protocol. (**E**) Two-feedback NF-κB signaling pathway showing IKK and the base module. (**F** and **G**) Computational analysis of existing (F) (*21*) and proposed (G) IKK structures. Heat maps [poor (red) to good (green)] represent the ability of the model to quantitatively fit the experimental data for a range of selected parameter values (table S5). A20 degradation rate (c4) was varied on a logarithmic scale two orders of magnitude above and below 0.0009 s^{-1}. The best fit is highlighted and the corresponding simulated N:C ratio shown (F and G, bottom) for all TNFα stimulation conditions; c4 = 0.00143 s^{-1} in (F) and c4 = 0.0045 s^{-1} in (G).

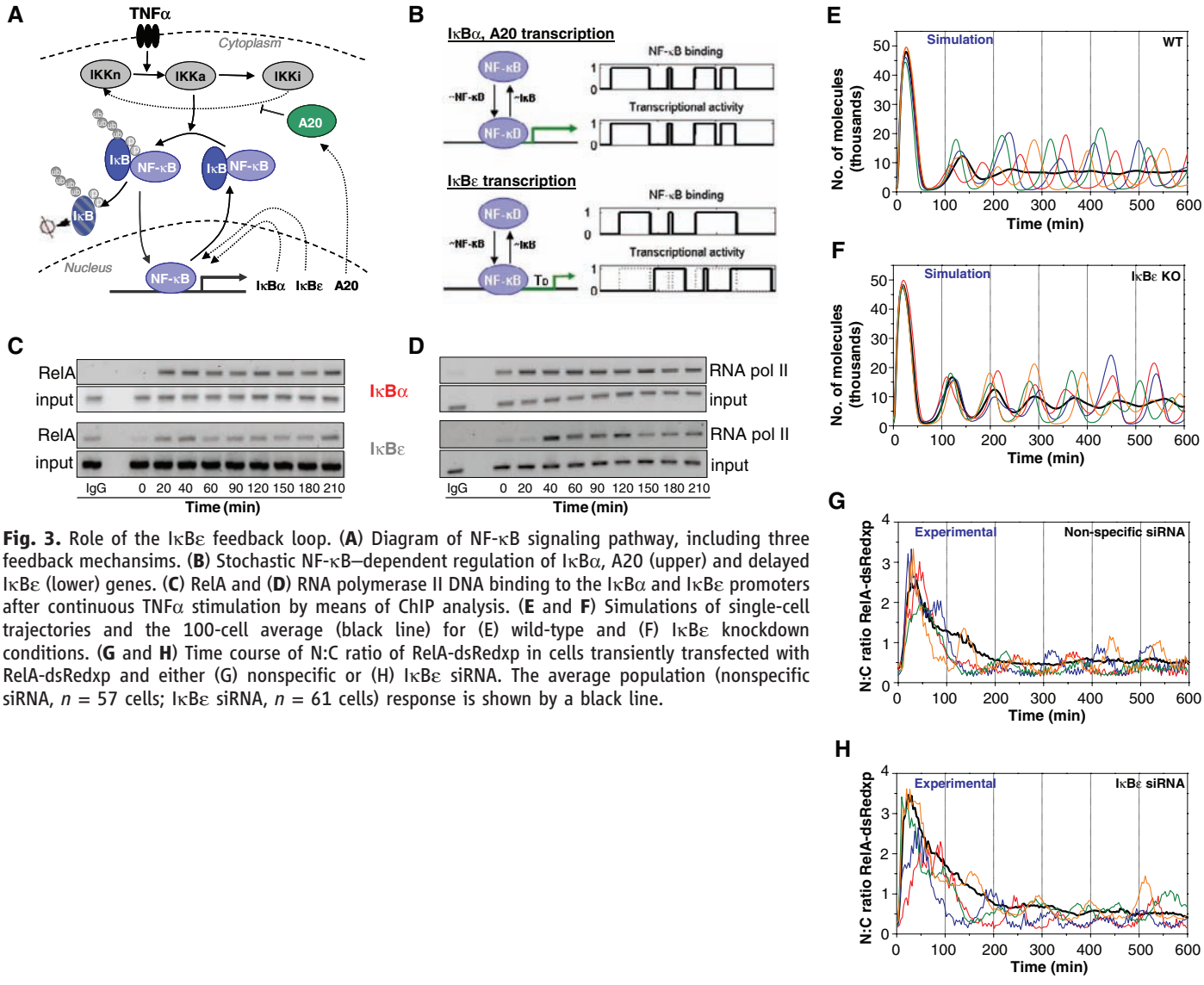

Fig. 3. Role of the IκBε feedback loop. (**A**) Diagram of NF-κB signaling pathway, including three feedback mechansims. (**B**) Stochastic NF-κB–dependent regulation of IκBα, A20 (upper) and delayed IκBε (lower) genes. (**C**) RelA and (**D**) RNA polymerase II DNA binding to the IκBα and IκBε promoters after continuous TNFα stimulation by means of ChIP analysis. (**E** and **F**) Simulations of single-cell trajectories and the 100-cell average (black line) for (E) wild-type and (F) IκBε knockdown conditions. (**G** and **H**) Time course of N:C ratio of RelA-dsRedxp in cells transiently transfected with RelA-dsRedxp and either (G) nonspecific or (H) IκBε siRNA. The average population (nonspecific siRNA, n = 57 cells; IκBε siRNA, n = 61 cells) response is shown by a black line.

the tested TNFα stimulation conditions demonstrated a need for model refinement (Fig. 2, E to G). We used the experimentally observed limited IκBα phosphorylation, which is associated with reduced NF-κB translocation level at higher pulse frequencies (Fig. 2, B and D), to constrain simulated IKK activity. The core NF-κB–IκBα network used a similar structure to that of previous models (Fig. 2E), although multiple model parameters were modified partly on the basis of cell-specific measurements (table S1). Model simulations using the existing IKK network structure (*14*) (Fig. 2F) failed to recapitulate experimental conditions because the repeated pulse stimulation required sufficient IKK activity to degrade almost all IκBα; however, persisting oscillations observed with continual TNFα were sensitive to high IKK activity (figs. S8 and S9). Using a scoring function to compare model performance with all experimental data (table S5), we composed a new deterministic model with a modified network structure of IKK and A20 NF-κB inhibitory protein interactions (Fig. 2G and fig. S10). The chosen model represented the simplest structure that included IKK state recycling (*15*) and was able to use a single parameter set to reproduce all of the experimental data. The A20 feedback loop was assumed to include other related negative feedback inhibitors, such as Cezanne (*16*) and Cylindromatosis (CYLD) (*17*), which together may limit the reactivation of IKK. The model predicted a low stability of A20, which could be compatible with a key regulatory factor being the ubiquitin-editing activity of A20 rather than its protein concentration. A20 activity may be linked to processes upstream of IKK (*18*), or IKK-mediated phosphorylation of A20 may inhibit IKK activity (*19*).

Persistent bulk cell oscillations have been observed after continuous TNFα by using EMSA assays of MEFs from IκBε-deficient or combined IκBε-IκBβ–deficient animals (*8*, *9*). Although deterministic simulation was appropriate for the work described above, the heterogeneous nature of single-cell responses to continuous TNFα stimulation in wild-type cells cannot be elucidated in this manner. Stochastic models (*20*, *21*) have been used to propose that cell-to-cell heterogeneity arises through intrinsic, stochastic, transcriptional variability because there are only two copies of the IκBα and A20 feedback genes (*21*). We developed a new hybrid, stochastic, three-feedback model on the basis of the deterministic model structure described above, which considered delayed stochastic transcription from the IκBε gene and stochastic transcription of the IκBα and A20 genes (Fig. 3, A and B). ChIP analysis confirmed that RelA binds to the IκBα and IκBε promoters in SK-N-AS cells within 20 min after TNFα stimulation (Fig. 3C). In contrast, RNA polymerase II was bound to the IκBα promoter before stimulation, whereas binding to the IκBε promoter was delayed (Fig. 3D), perhaps as a result of chromatin remodeling. The three-feedback stochastic model predicted persistent oscillations of similar amplitude in both wild-type (Fig. 3E) and IκBε-deficient (Fig. 3F) cells after stimulation. Furthermore, stochastic variation from delayed IκBε feedback may generate enhanced cell-to-cell heterogeneity

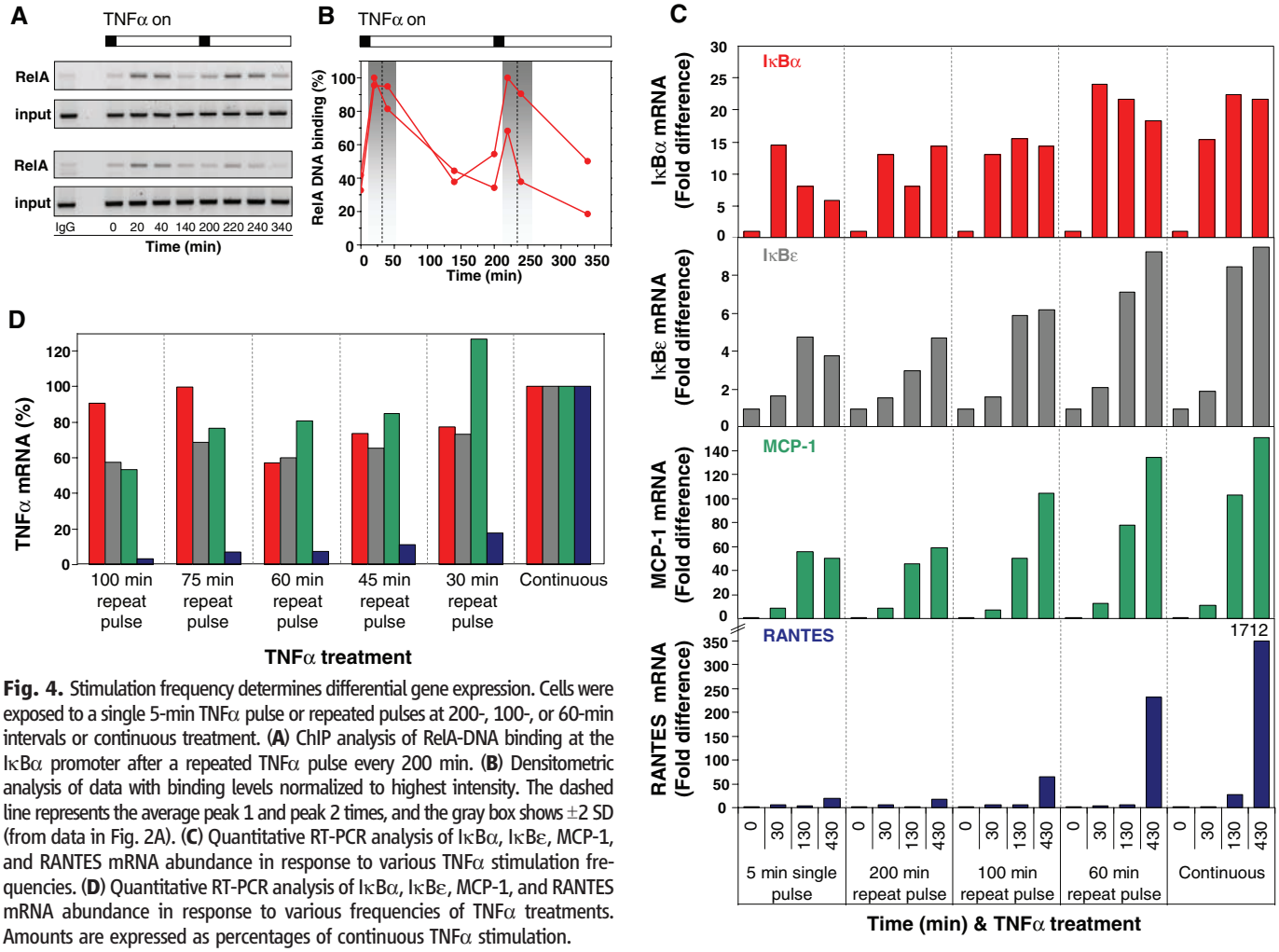

Fig. 4. Stimulation frequency determines differential gene expression. Cells were exposed to a single 5-min TNFα pulse or repeated pulses at 200-, 100-, or 60-min intervals or continuous treatment. (**A**) ChIP analysis of RelA-DNA binding at the IκBα promoter after a repeated TNFα pulse every 200 min. (**B**) Densitometric analysis of data with binding levels normalized to highest intensity. The dashed line represents the average peak 1 and peak 2 times, and the gray box shows ±2 SD (from data in Fig. 2A). (**C**) Quantitative RT-PCR analysis of IκBα, IκBε, MCP-1, and RANTES mRNA abundance in response to various TNFα stimulation frequencies. (**D**) Quantitative RT-PCR analysis of IκBα, IκBε, MCP-1, and RANTES mRNA abundance in response to various frequencies of TNFα treatments. Amounts are expressed as percentages of continuous TNFα stimulation.

in wild-type cells as compared with that in IκBε-deficient cells. The lack of IκBε feedback could therefore generate increased cell-to-cell homogeneity, which was predicted to be detectable as oscillations at the average population level (Fig. 3F). Experimental small interfering RNA (siRNA) depletion of IκBε feedback in SK-N-AS cells (Fig. 3H) had no effect on oscillation amplitude (Fig. 3G), which contradicts the prediction that IκBε feedback might dampen oscillations in wild-type cells (*9*). Although IκBε-deficient MEFs showed homogeneous cell-to-cell oscillations, the stochastic three-feedback model predicted that this effect would not occur in cells overexpressing RelA by as little as twofold [as in our siRNA knockdown experiments (fig. S15)]. Therefore, the three-feedback stochastic model was able to simulate and predict key aspects of the available experimental data.

To assess the functional importance of oscillation timing in TNFα-induced NF-κB signaling in single cells, we used quantitative reverse transcription polymerase chain reaction (RT-PCR) to measure the time course of transcription from a set of early, middle, and late NF-κB–dependent endogenous genes in response to various durations and frequencies of TNFα treatment. ChIP analyses after repeated 100- and 200-min pulses showed cycles of DNA binding (Fig. 4, A and B, and fig. S23). Over a 430-min time course, we observed successively later peaks in the mRNA transcription of four representative genes in response to TNFα stimulation (from early to late: IκBα, IκBε, MCP-1, RANTES) (Fig. 4C) (*8*, *22*). Although IκBα responded equally to a 5-min single pulse of TNFα and to pulses at 200-min intervals, later genes showed reduced responses, and the gene encoding the RANTES chemokine exhibited almost no response. There was an increase in late transcript abundance in which stimuli were applied at 100-min intervals, which was even more marked when the cells were stimulated at shorter intervals (Fig. 4D). Thus, varying frequencies of NF-κB nuclear entry result in the differential regulation of particular downstream genes.

In this study, we used combined experimental and computational studies to explain the source of cellular heterogeneity and show that oscillations are an important characteristic of the response of NF-κB to TNFα. Cells in inflammatory tissues may experience varying cytokine stimulation. In response to timed fluctuations in TNFα stimulation, the NF-κB response can become homogeneous and can be driven at differing frequencies. Such varying frequencies in stimulation resulted in altered gene-expression profiles, specifically affecting the abundance of late gene transcription. These results therefore support the idea of oscillatory dynamics having a key functional role in this important stress-response system. The recent observation that the yeast calcium–regulated transcription factor Crz1 also controls gene expression through nuclear translocation frequency (*23*) suggests that this behavior may be a property of other important signaling pathways, such as p53 (*24*).

References and Notes

1. M. S. Hayden, S. Ghosh, *Cell* **132**, 344 (2008).
2. A. Hoffmann, D. Baltimore, *Immunol. Rev.* **210**, 171 (2006).
3. N. D. Perkins, *Nat. Rev. Mol. Cell Biol.* **8**, 49 (2007).
4. D. E. Nelson *et al.*, *Science* **306**, 704 (2004).
5. M. J. Berridge, M. D. Bootman, H. L. Roderick, *Nat. Rev. Mol. Cell Biol.* **4**, 517 (2003).
6. S. Friedrichsen *et al.*, *Endocrinology* **147**, 773 (2006).
7. D. E. Nelson *et al.*, *Science* **308**, 52b (2005).
8. A. Hoffmann, A. Levchenko, M. L. Scott, D. Baltimore, *Science* **298**, 1241 (2002).
9. J. D. Kearns, S. Basak, S. L. Werner, C. S. Huang, A. Hoffmann, *J. Cell Biol.* **173**, 659 (2006).
10. D. Barken *et al.*, *Science* **308**, 52a (2005).
11. M. W. Covert, T. H. Leung, J. E. Gaston, D. Baltimore, *Science* **309**, 1854 (2005).

12. S. L. Werner, D. Barken, A. Hoffmann, *Science* **309**, 1857 (2005).
13. A. E. Ihekwaba *et al.*, *Syst. Biol. (Stevenage)* **152**, 153 (2005).
14. T. Lipniacki, P. Paszek, A. R. Brasier, B. Luxon, M. Kimmel, *J. Theor. Biol.* **228**, 195 (2004).
15. H. Hacker, M. Karin, *Sci. STKE* **2006**, re13 (2006).
16. K. Enesa *et al.*, *J. Biol. Chem.* **283**, 7036 (2008).
17. E. Trompouki *et al.*, *Nature* **424**, 793 (2003).
18. S. C. Sun, *Nat. Rev. Immunol.* **8**, 501 (2008).
19. J. E. Hutti *et al.*, *Mol. Cell. Biol.* **27**, 7451 (2007).
20. F. Hayot, C. Jayaprakash, *J. Theor. Biol.* **240**, 583 (2006).
21. T. Lipniacki, P. Paszek, A. R. Brasier, B. A. Luxon, M. Kimmel, *Biophys. J.* **90**, 725 (2006).
22. B. Tian, D. E. Nowak, A. R. Brasier, *BMC Genomics* **6**, 137 (2005).
23. L. Cai, C. K. Dalal, M. B. Elowitz, *Nature* **455**, 485 (2008).
24. G. Lahav *et al.*, *Nat. Genet.* **36**, 147 (2004).
25. We thank N. Perkins for reading the manuscript and D. Jackson, M. Kimmel, and T. Lipniacki for discussion. The work was supported by Biotechnology and Biological Sciences Research Council (BBSRC) grants BBD0107481, BBF0059381, BBC0082191, and BBC0071581; BBSRC studentships to L.A. and K.S. (AstraZeneca Collaborative Awards in Science and Engineering); and Medical Research Council grant G0500346. C.V.H. holds a Professor John Glover Memorial Research Fellowship; D.A.R. held an Engineering and Physical Sciences Research Council Senior Fellowship [EP/C544587/1, GR/S29256/01 and European Union (BioSim Network contract 005137)]; D.B.K. holds a Royal Society/Wolfson Merit Award; and V.S. holds a BBSRC David Phillips Research Fellowship (BBC5204711). Hamamatsu Photonics and Carl Zeiss Limited provided training and technical support.

Supporting Online Material

www.sciencemag.org/cgi/content/full/324/5924/242/DC1
Materials and Methods
Figs. S1 to S32
Tables S1 to S8
References

19 August 2008; accepted 29 December 2008
10.1126/science.1164860

Antibody Recognition of a Highly Conserved Influenza Virus Epitope

Damian C. Ekiert,[1] Gira Bhabha,[1] Marc-André Elsliger,[1] Robert H. E. Friesen,[2] Mandy Jongeneelen,[2] Mark Throsby,[2] Jaap Goudsmit,[2] Ian A. Wilson[1,3]*

Influenza virus presents an important and persistent threat to public health worldwide, and current vaccines provide immunity to viral isolates similar to the vaccine strain. High-affinity antibodies against a conserved epitope could provide immunity to the diverse influenza subtypes and protection against future pandemic viruses. Cocrystal structures were determined at 2.2 and 2.7 angstrom resolutions for broadly neutralizing human antibody CR6261 Fab in complexes with the major surface antigen (hemagglutinin, HA) from viruses responsible for the 1918 H1N1 influenza pandemic and a recent lethal case of H5N1 avian influenza. In contrast to other structurally characterized influenza antibodies, CR6261 recognizes a highly conserved helical region in the membrane-proximal stem of HA1 and HA2. The antibody neutralizes the virus by blocking conformational rearrangements associated with membrane fusion. The CR6261 epitope identified here should accelerate the design and implementation of improved vaccines that can elicit CR6261-like antibodies, as well as antibody-based therapies for the treatment of influenza.

Over the past century, three human influenza A pandemics (1918 H1N1 Spanish, 1957 H2N2 Asian, and 1968 H3N2 Hong Kong) have killed ~50 million to 100 million people worldwide. Each pandemic virus was derived, at least in part, from an avian influenza virus by direct interspecies transmission or exchange of genetic material between avian and human viruses (*1*–*4*). In each case, an HA envelope glycoprotein was acquired that was antigenically distinct from the HAs of the human viruses in circulation at that time. HA is the primary target of neutralizing antibodies and rapidly and continuously accumulates mutations to escape recognition by the immune system. In pandemic years, HAs are shuffled from the vast reservoir of 16 HA subtypes in avian viruses into a circulating human virus to evade prevailing immunity in the human population. Thus, although many factors likely contribute to virulence and transmissibility, immune evasion is critical for the rapid spread of pandemic and epidemic viruses.

Several small molecules are in use for treatment of influenza. Most notable are neuraminidase (NA) inhibitors, oseltamivir (Tamiflu) and zanamivir (Relenza), which prevent release of nascent virions, and amantadine (*5*), which interferes with the M2 channel proton conducting activity. However, excessive use leads to resistant viruses (*6*–*8*) that often show surprisingly little attenuation from the escape mutations, thereby contributing to rapid spread worldwide (*6*). Recently, a binding pocket was characterized on the HA for the fusion inhibitor tert-butyl hydroquinone (TBHQ) (*9*), which shows great promise but is still in the early stages of development. Consequently, vaccination remains the most effective countermeasure against influenza virus.

Current trivalent influenza vaccines elicit a potent neutralizing antibody response to the vaccine strains and closely related isolates but rarely extend to more diverged strains within a subtype or to other subtypes (*10*). Selection of the appropriate vaccine strains presents many challenges and frequently results in suboptimal protection (*11*, *12*). Furthermore, predicting the subtype and clade of the next pandemic virus, including when and where it will arise, is currently impossible. A vaccine that stimulates production of antibodies capable of neutralizing multiple influenza A subtypes would eliminate much of the guesswork associated with strain selection and impede emerging pandemic viruses. Although a few rare antibodies with broad, heterosubtypic patterns of neutralization have been reported, their epitopes remain obscure and have hampered attempts at rational vaccine design (*13*–*15*).

Antibody CR6261 was isolated from the immune repertoire of a healthy, vaccinated individual by using phage display selection on recombinant H5 HA (*15*). Despite no known exposure to H5 viruses, several clones capable of neutralizing H5 viruses were obtained. Human immunoglobulin G1 (IgG1) CR6261 neutralizes multiple influenza subtypes, including H1, H2, H5, H6, H8, and H9, and protects mice from lethal challenge with H1N1 and H5N1 viruses when administered up to 5 days postinfection (*15*). To characterize the CR6261 epitope on the HA and the mechanism of neutralization, we determined crystal structures of CR6261 Fab in complex with HAs from the human 1918 H1N1 pandemic virus (A/South Carolina/1/1918; SC1918/H1) and from a highly pathogenic avian H5N1 virus (A/Vietnam/1203/2004; Viet04/H5).

The SC1918/H1 and Viet04/H5 HA ectodomains were expressed in baculovirus, and Fab CR6261 was expressed in mammalian cells (*16*). Cocrystal structures were determined at 2.2 Å and 2.7 Å resolution by molecular replacement (table S1) (*17*) and revealed three antibodies bound per HA trimer (Fig. 1). Both HAs are very similar to their unliganded structures (fig. S1) (*18*–*20*). Each HA polypeptide is proteolytically cleaved during viral maturation to two disulfide-linked chains, HA1 and HA2. HA1 consists primarily of the membrane-distal receptor binding and vestigial esterase domains, but its N- and C-terminal regions extend toward the viral membrane and are intertwined with the exterior surface of HA2. HA2 constitutes the core fusion machinery in the stalk region and is dominated by the long, central CD helix (residues 75 to 126) that forms a trimeric coiled-coil and the shorter A helix (residues 38 to 58) that packs against the central helical bundle (*21*). Exposure to low pH leads to major structural rearrangements in HA2 that facilitate membrane fusion (*22*, *23*).

[1]Department of Molecular Biology, The Scripps Research Institute, 10550 North Torrey Pines Road, La Jolla, CA 92037, USA. [2]Crucell Holland BV, Archimedesweg 4-6, 2301 CA Leiden, Netherlands. [3]The Skaggs Institute for Chemical Biology, The Scripps Research Institute, 10550 North Torrey Pines Road, La Jolla, CA 92037, USA.

*To whom correspondence should be addressed. E-mail: wilson@scripps.edu